Journal of Materials Chemistry A

Accepted Manuscript

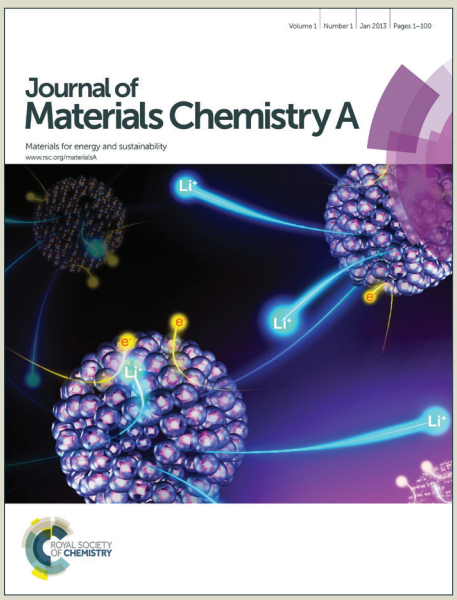

This is an *Accepted Manuscript*, which has been through the Royal Society of Chemistry peer review process and has been accepted for publication.

Accepted Manuscripts are published online shortly after acceptance, before technical editing, formatting and proof reading. Using this free service, authors can make their results available to the community, in citable form, before we publish the edited article. We will replace this *Accepted Manuscript* with the edited and formatted *Advance Article* as soon as it is available.

You can find more information about *Accepted Manuscripts* in the Information for Authors.

Please note that technical editing may introduce minor changes to the text and/or graphics, which may alter content. The journal's standard Terms & Conditions and the Ethical guidelines still apply. In no event shall the Royal Society of Chemistry be held responsible for any errors or omissions in this *Accepted Manuscript* or any consequences arising from the use of any information it contains.

ROYAL SOCIETY OF CHEMISTRY

www.rsc.org/materialsA

Journal of Materials Chemistry A

Dynamic Article Links ►

Cite this: DOI: 10.1039/c0xx00000x

ARTICLE TYPE

www.rsc.org/xxxxxx

Coral-Like Film of Ni@NiS with Core-Shell Particles for the Counter Electrode of an Efficient Dye-Sensitized Solar Cell

Hui-Min Chuang,[a,+] Chun-Ting Li,[a,+] Min-Hsin Yeh,[a] Chuan-Pei Lee,[a] R.Vittal,[a] and Kuo-Chuan Ho[a,b,*]

Received (in XXX, XXX) Xth XXXXXXXXX 20XX, Accepted Xth XXXXXXXXX 20XX
DOI: 10.1039/b000000x

A coral-like film of nickel@nickel sulfide (Ni@NiS) was obtained on a conducting glass through an electrochemical method, in which the Ni functioned as a template. Three types of Ni thin films were electrodeposited on fluorine-doped tin oxide (FTO) substrates by pulse current technique at the passed charge densities of 100, 200, and 300 mC/cm^2, which rendered custard apple-like, coral-like, and cracked nanostructures, respectively. Subsequently, nickel sulfide films were coated on these Ni films by using pulse potential technique. Due to the template effect of the Ni films, the composite films of Ni@NiS also assumed the same structures as those of their nickel templates. In each case of the films the particle of the film assumed a core-shell structure. The Ni@NiS coated FTO glasses were used as the counter electrodes for dye-sensitized solar cells (DSSCs). The DSSC with the coral-like Ni@NiS film on its counter electrode exhibits the highest power conversion efficiency (η) of 7.84%, while the DSSC with platinum film on its counter electrode shows an η of 8.11%. The coral-like Ni@NiS film exhibits multiple functions, *i.e.,* large surface area, high conductivity, and great electrocatalytic ability for iodine/triiodine (I^-/I_3^-) reduction. X-ray photoelectron spectroscopy (XPS), X-ray diffraction pattern (XRD), scanning electron microscopy (SEM), and four-point probe technique were used to characterize the films. The photovoltaic parameters are substantiated using incident photon–to–current conversion efficiency (IPCE) curves, cyclic voltammetry (CV), electrochemical impedance spectroscopy (EIS), and Tafel polarization plots. The IPCE curves were further used to calculate theoretical short-current densities of the cells.

Introduction

Currently, nanoscale materials have been widely used for electrochemical studies[1,2]. Their outstanding performance has attracted many researchers to further study their properties and find new procedures. The advantages of nanoscale materials lie in their fast and simple preparation methods, enhanced electrical properties, and, most importantly, variable nanoscale morphology[3-5]. Nanostructural cores can provide not only large surface area, but also one-dimensional (1D) or two-dimensional (2D) electron transfer pathways for the target shell materials[6-8]. Nanostructural materials are usually prepared via nano-templates through the following steps: (1) synthesizing the specific nano-template on a substrate, (2) coating the target material on the surface of the template, and (3) removing the template[9]. Unfortunately, removal of the template often causes a huge damage for the target material at the same time. In some cases the template need not be removed and it can act as a multi-functional template, *i.e.,* with great conductivity, large effective surface area, and good electrochemical properties[10]. Metallic nickel (Ni) has been widely studied in many electrochemical devices, *e.g.,* dye-sensitized solar cells (DSSCs)[11], because of its abundance in content, outstanding conductivity, and electrochemical properties. Joshi *et al.* have obtained, through a thermal decomposition process, a film of nickel incorporated carbon nanotube/nanofiber (Ni-CNT-CNF) on FTO glass, and employed the thus obtained FTO glass as the counter electrode in a dye-sensitized solar cell[12]. Bajpai *et al.* have developed a platinum free counter electrode for DSSCs using graphene platelets (GP) supported nickel nanoparticles (NPs) as the active catalyst[13]. In their study, nickel nanoparticles were reported to enhance electronic conductivity and electrocatalytic ability for the counter electrode. Ni nano-templates have also been used in various other electrochemical devices, *e.g.,* sensors[14-17], capacitors[18-21], catalysts[22], and energy storage[23], intending always to improve their performance.

DSSCs have been developed since 1991[24], and caught intensive attention from several research groups, owing to their advantages, such as simple and low–cost production and high light–to–electricity conversion efficiencies. A DSSC consists of three important parts: titanium dioxide (TiO_2) film adsorbed with a sensitizer (dye) as the photoanode, electrolyte, and counter electrode (CE). Among these, counter electrode plays an important role to trigger the reduction of triiodide ions in the

Journal of Materials Chemistry A Accepted Manuscript

electrolyte. Platinum (Pt) is the most popular catalytic material on the CE, but its high cost and rarity make it difficult to be used in large amounts[25,26]. Several substitute materials have been widely investigated to replace Pt, or at least, to reduce the cost for the preparation of CEs[27-29]. Recently, a number of studies have shown that transition metal compounds bestow to the counter electrode's high electrical conductivity, good electrocatalytic ability for I_3^- reduction, and admirable stability. To reduce the cost and thereby enlarge the production scale of the DSSCs, transition metal carbides (TMCs), nitrides (TMNs), sulfides (TMSs), seleniums (TMSes), phosphide (TMPs) and oxides (TMOs) have been widely studied as the counter electrode materials[30-34]. Ni-based compounds are promising electrocatalytic materials for counter electrodes, owing to their excellent electrocatalytic ability. Guai *et al*. obtained a sulfur-doped nickel oxide thin film on the counter electrode substrate of a DSSC, applying an electrophoretic deposition method, and obtained a cell efficiency (η) of 5.04%[35]. Dou *et al*. synthesized a composite film of nickel phosphide-embedded graphene on the CE of a DSSC, using a hydrothermal process, and attained an η of 5.70%[36]. Sun *et al.* used a nickel sulfide (NiS) thin film as the catalyst for the CE of a DSSC and realized an efficiency of 6.83%, while obtaining an efficiency of 7% for the DSSC with platinum film on its counter electrode[37]. Gong *et al*. synthesized $Ni_{0.85}Se$ particles as the catalytic material for the counter electrode of a DSSC and realized a high power conversion efficiency of 8.32% for the DSSC[10]. Ku *et al.* used NiS as the catalytic material on the counter electrode of a DSSC and also used a new electrolyte with thiolate/disulfide redox couple; the pertinent DSSC exhibited an admirable efficiency of 6.25%, while its platinum counterpart showed an η of only 3.98%.[38]

In this study, we deposited a coral-like composite film of Ni and NiS on a fluorine-doped tin oxide (FTO) glass, in which the particles of the film had a core of nickel and a shell of nickel sulfide. Here, metallic Ni was first deposited by a pulse current technique with a charge density of 200 mC/cm^2 and then NiS was deposited on it by a pulse potential technique. The first layer of nickel functioned as a template and enabled a coral-like structure for the composite film of nickel and nickel sulfide. The thus coated FTO substrate was used as the counter electrode for a DSSC. This DSSC exhibited a power conversion efficiency of 7.84%, while its counterpart DSSC with platinum film on its counter electrode showed an η of 8.11%. By applying the charge densities of 100 and 300 mC/cm^2 for the deposition of nickel, power conversion efficiencies of 7.28% and 7.29% were obtained, respectively, for the DSSCs with the corresponding NiS composite films. It is to be noted that all the cells performed better than that with bare nickel sulfide on its counter electrode. After extensive literature search, it was found that this (7.84%) is the highest power conversion efficiency for any DSSC using NiS as the counter electrode material. Ni@NiS is much cheaper than platinum, and can therefore be further explored to replace the expensive platinum as the catalytic film for the counter electrode of a DSSC.

Experimental

Materials

Titanium (IV) tetraisoproproxide (TTIP, >98%), ethanol (EtOH, 99.5%), isopropyl alcohol (IPA, 99.5%), lithium perchlorate (LiClO4, ≥98.0%), thiourea (≥99.0%), 1-butyl-3-methyl imidazolium iodide (BMII), 1-ethyl-3-methy imidazolium tetrafluoroborate ($EMIBF_4$), and 2–methoxyethanol (≥99.5%) were obtained from Sigma Aldrich. Lithium iodide (LiI, synthetical grade), iodine (I2, synthetical grade), and poly(ethylene glycol) (PEG, MW~20,000) were procured from Merck. Acetone (99+%), 4–tert–butylpyridine (TBP, 96%), and tert–butyl alcohol (TBA, 96%) were received from Acros. 3–methoxypropionitrile (MPN, 99%) was purchased from Fluka. 1,2–dimethyl–3–propylimidazolium iodide (DMPII), cis-diisothiocyanato-bis(2,2'-bipyridyl-4,4'-dicarboxylato)ruthenium (II) bis (tetra-butylammonium) (N719 dye), TiO_2 paste for transparent layer (TL paste, *i.e.*, Ti-nanoxide HT/SP, 13 nm), and 60 μm-thick Surlyn® film (SX1170-60) were supplied by Solaronix (S.A., Aubonne, Switzerland). Acetonitrile (ACN, 99.99%) and nitric acid (HNO_3, *ca.* 65% solution in water) were acquired from J. T. Baker. Nickel (II) sulfate hexahydrate ($NiSO_4 \cdot 6H2O$) was bought from Showa. Nickel (II) chloride hexahydrate ($NiCl_2 \cdot 6H_2O$, 98%) was got from Alfa Aesar. Commercial light scattering TiO_2 particles, ST-41 with 200 nm, were obtained from Ishihara Sangyo, Ltd., Japan.

Preparation of various CEs

The platinum counter electrode was prepared by sputtering Pt on an FTO glass (10 Ω sq.$^{-1}$, UR-ITO007-0.7mm, Uni-onward Corp., Taiwan) for a thickness of 50 nm. Bare nickel sulfide film and the composite film of nickel and nickel sulfide were electrodeposited by using a potentiostat/galvanostat. (PGSTAT 30, Autolab, Eco-Chemie, the Netherlands). A cleaned FTO glass (1 cm^2) was used as the working electrode, and a Pt foil and Ag/AgCl were used as the counter and reference electrodes, respectively. First of all, the Ni first layer, *i.e.*, the template, was obtained on the FTO glass by pulse current technique in an aqueous deposition bath of 0.025 M $NiSO_4$ and 0.975 M $LiClO_4$. Each cycle of pulse current consisted of an anodic current density of 0 mA/cm^2 for 10 s and a cathodic current density of 0.25 mA/cm^2 for 20 s. We applied 20 cycles, 40 cycles, and 60 cycles, corresponding to charge densities of 100 mC/cm^2, 200 mC/cm^2, and 300 mC/cm^2, so as to prepare 100-Ni, 200-Ni, and 300-Ni nanotemplate thin films, respectively. Nickel sulfide layers were then deposited onto the Ni templates by pulse potential deposition in an aqueous deposition bath of 50.0 mM $NiCl_2$•$6H_2O$ and 1.0 M thiourea. Each cycle of pulse potential deposition consisted of a cathodic bias of -0.9 V for 6 sec and an anodic bias of 0.1 V for 24 s. We applied the same 10 cycles to deposit the NiS layers onto the Ni templates of 100-Ni, 200-Ni, and 300-Ni to ultimately obtain three kinds of Ni@NiS composite films, designated as 100-Ni@NiS, 200-Ni@NiS, and 300-Ni@NiS, respectively. As for the counter electrode with bare NiS, we applied the same 10 cycles under pulse potential deposition.

Fabrication of DSSCs

A TiO_2 colloid was obtained by adding 72 ml of TTIP to 430 ml of 0.1 M aqueous nitric acid with constant stirring at 88 °C for 8 h. After that, the colloid was cooled down to room temperature, transferred into an autoclave (PARR 4540, U.S.A.), and heated at 240 °C for 12 h, in order to allow the TiO_2 nanoparticles to grow uniformly (*ca.* 20 nm). Then the autoclaved–TiO_2 colloid was

Journal of Materials Chemistry A Accepted Manuscript

This journal is © The Royal Society of Chemistry [year]

concentrated to contain 8 wt% of TiO_2 nanopaticles. The TiO_2

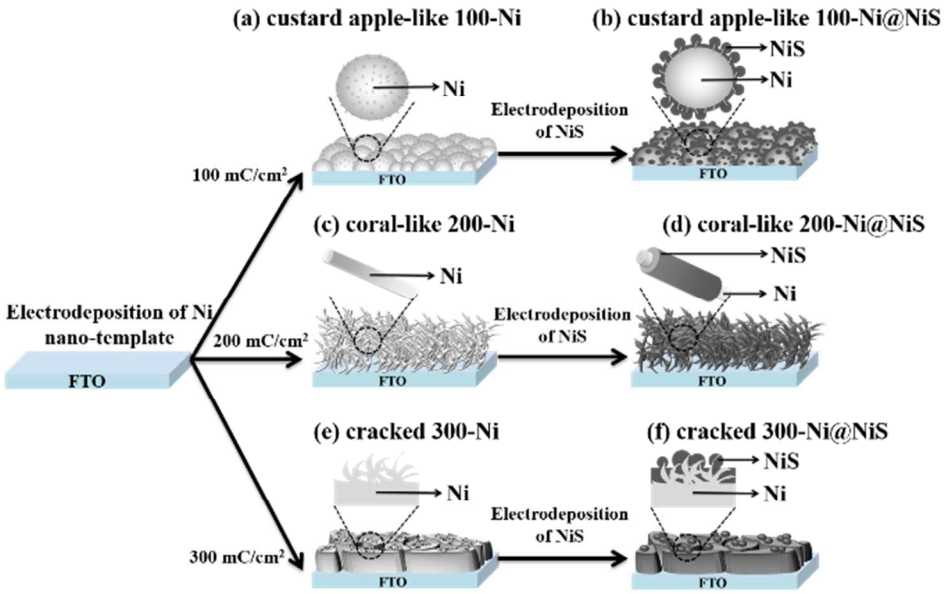

Scheme 1. Synthesis of Ni@NiS composite films on FTO glass. The scheme shows the template structures of Ni at different charge densities, and their corresponding NiS composite films. It is to be noted that in each case the particle of the composite film assumes a core-shell structure.

paste for scattering layer (SL paste) was prepared by adding 25 wt% of PEG and 100 wt% of ST-41 (with respect to the weight of TiO_2 nanoparticles) into the TiO_2 colloid.

The TiO_2 photoanode was prepared by using the TL paste and SL paste mentioned above. FTO conducting glass was first cleaned with a neutral cleaner and then washed with deionized water, acetone, and isopropanol sequentially. The conducting surface of the FTO was treated with a solution of TTIP in 2–methoxyethanol (weight ratio of 1:3) for obtaining a TiO_2 compact layer. The FTO glass was gradually heated to 450 °C and maintained at the same temperature for 30 min. The compact layer is required, because a good mechanical contact will be obtained between the substrate and the TiO_2 transparent layer in the DSSC, and also the conducting surface of the FTO substrate will be isolated from the electrolyte in the DSSC. Ten micrometers of a transparent TiO_2 layer was first coated on the treated FTO glass, using the TiO_2 paste for transparent layer (TL paste). Five micrometers of a scattering layer was then coated on the transparent layer, using the TiO_2 paste for scattering layer (SL paste). Thus the total film thickness was 15 micrometers. The coated FTO glass was sintered at 500 °C for 30 min in an air atmosphere. After the sintering process, the TiO_2 film was shaved to obtain an active area of 0.4 × 0.4 cm^2. Then it was immersed for 24 h in 5×10^{-4} M N719 dye solution at room temperature. The N719 dye was dissolved in ACN and tBA (volume ratio of 1:1) to obtain the standard dye solution. The photoanode was coupled with the CE, and these two electrodes were separated by a 60 μm–thick Surlyn® film (SX1170–60, Solaronix S.A., Aubonne, Switzerland) and sealed together by heating. The electrolyte, which contained 0.1 M LiI, 0.6 M DMPII, 0.05 M I_2, and 0.5 M TBP in MPN/ACN (volume ratio = 1:1), was injected into the gap between these two electrodes by capillarity.

For further investigation for the long-term stability of the DSSCs, the binary ionic-liquid-based electrolyte composed of 0.2 M I2 and 0.5 M TBP were added in a mixture of BMII/EMIBF4 (volume ratio = 65/35). The ionic-liquid-based electrolyte penetrated slowly into the gap between the photoanode and CE through the electrolyte-injecting hole, which was previously made onto the counter electrode with a drilling machine, and the hole was sealed with hot-melt glue after the fully filling of the electrolyte.

Characterization of CEs and DSSCs

Surface morphologies of films of Pt, Bare NiS, and composite Ni@NiS were observed by a field–emission scanning electron microscope (FE–SEM, Nova NanoSEM 230, FEI, Oregon, USA). Surface chemical analyses of various films were made by X-ray photoelectron spectroscopy (XPS, Thermo Scientific Theta Probe, UK). Photovoltaic parameters of the DSSCs were obtained by a potentiostat/galvanostat (PGSTAT 30, Autolab, Eco–Chemie, Utrecht, the Netherlands), under 100 mW cm^{-2}. The DSSCs were illuminated by a class A quality solar simulator (XES–301S, AM1.5G, San–Ei Electric Co., Ltd., Osaka, Japan) and the incident light intensity (100 mW cm^{-2}) was calibrated with a standard Si cell (PECSI01, Peccell Technologies, Inc.). IPCE curves of the DSSCs were obtained by the potentiostat/galvanostat and by another class A quality solar simulator (PEC–L11, AM1.5G, Peccell Technologies, Inc., Kanagawa, Japan) equipped with a monochromator (model 74100, Oriel Instrument, California, USA). The incident radiation flux (φ) was obtained by using an optical detector (model 71580, Oriel Instrument, California, USA) and a power meter (model 70310, Oriel Instrument, California, USA).

Catalytic abilities of the CEs with various films for I^-/I_3^- redox couple could be estimated by cyclic voltammetry (CV), Tafel plots, and electrochemical impedance spectroscopy (EIS). Cyclic voltammetry (CV) was performed by a potentiostat/galvanostat using a three–electrode system in an ACN-based solution, containing 10.0 mM I^-, 1.0 mM I_2, and 0.1 M $LiClO_4$. In the CV

Journal of Materials Chemistry A Accepted Manuscript

experiments, platinum, Bare NiS, and Ni@NiS composite films were used as the working electrodes, and a Pt foil and an Ag/Ag^+ electrode were used as the counter and reference electrodes, respectively. Symmetric cells were used for obtaining Tafel plots and EIS spectra. The symmetric cell consisted of two identical electrodes, *i.e.*, identical Pt, Bare NiS, or Ni@NiS electrodes. All these measurements were performed by using the potentiostat/galvanostat, equipped with an FRA2 module under a constant light illumination of 100 mW cm^{-2}. The frequency range explored was 10 mHz to 65 kHz.

Results and discussion

Structural characterization of various counter electrode films

X-ray photoelectron spectroscopy (XPS) was used to analyze chemical bindings and elemental ratios in the films of Ni, NiS, and Ni@NiS. The Ni templates were synthesized by controlling the charge densities at 100, 200, 300 mC/cm^2, and therefore these templates are denoted as 100-Ni, 200-Ni, and 300-Ni, respectively. In Fig. 1a to 1c, the XPS spectra of 100-Ni, 200-Ni, and 300-Ni all show two peaks at 852.8 and 874.2 eV, corresponding to Ni $2p_{3/2,\,sat}$ and Ni $2p_{1/2,\,sat}$ orbitals, respectively, thereby referring to pure Ni metal; there are no other peaks referring to the impurity of NiO. Thus, we confirm that pure Ni metal layers were successfully prepared through the technique of pulse current deposition. Nickel sulfide layers were coated on the 100-Ni, 200-Ni, and 300-Ni templates to obtain Ni@NiS composite films. The Ni@NiS composite films formed with 100-Ni, 200-Ni, and 300-Ni templates are denoted as 100-Ni@NiS, 200-Ni@NiS, and 300-Ni@NiS, respectively. A bare NiS film was also coated directly on a fluorine-doped tin oxide (FTO) substrate. As shown in Fig. 2a to 2d, the XPS spectra of Bare NiS, 100-Ni@NiS, 200-Ni@NiS, and 300-Ni@NiS, all show three peaks, indicating the S-Ni bindings at 162.6 and 225.3 eV, and Ni-S binding at 854.9 eV, corresponding to S $2p_{3/2}$, S 2s, and Ni $2p_{3/2}$ orbitals, respectively. The computer data of XPS also showed the stoichiometric atomic ratio of Ni to S to be 1:1.

X-ray diffraction (XRD) spectroscopy was employed to investigate the composition of a film of Ni@NiS. In Fig. 3, the crystalline phase of NiS can be observed at 34.82°, according to the Joint Committee on Powder Diffraction Standards (JCPDS card No. 3-1149). The crystalline phase of Ni can be observed at 45.42°, which corresponding to the data in JCPDS card No. 88-2326. From this XRD data, it can be confirmed that the Ni@NiS composite film consists of nickel and nickel sulfide. It will be seen soon that nickel has functioned as the template for NiS; that is to say, they are not bilayers.

A field-emission scanning electron microscope (FE-SEM) was employed to observe the microstructure of the films. FE–SEM images of the films are shown in Fig. 4, which also includes the image of a platinum film and of a NiS film. Scheme 1 shows the synthesis of Ni@NiS composite films on FTO glass. The scheme shows the template structures of Ni at different charge densities, and their corresponding Ni@NiS composite films. It is to be noted that in each case the particle of the composite film assumes a core-shell structure.

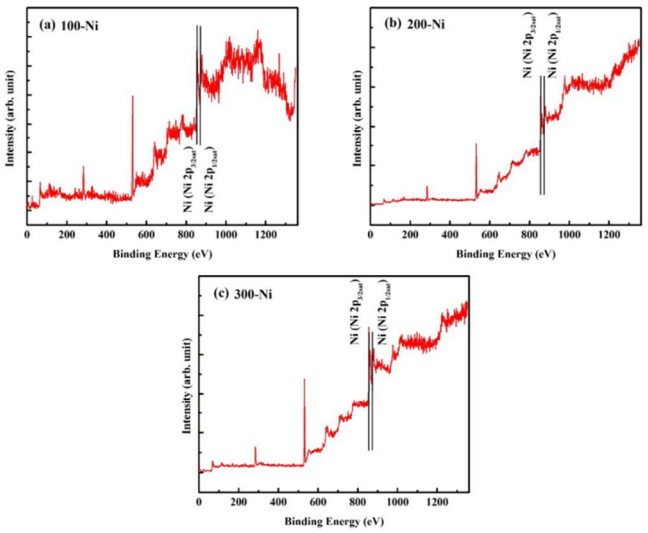

Fig. 1 XPS of films of (a) 100-Ni, (b) 200-Ni, and (c) 300-Ni.

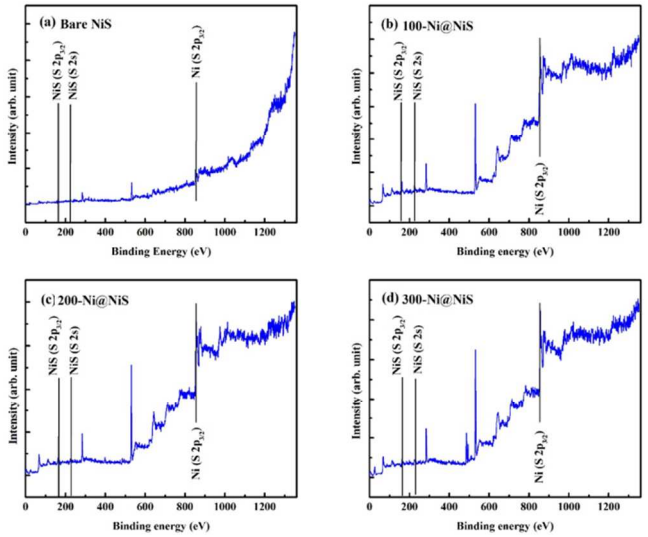

Fig. 2 XPS of the films of (a) Bare NiS, (b) 100-Ni@NiS, (c) 200-Ni@NiS, and (d) 300-Ni@NiS.

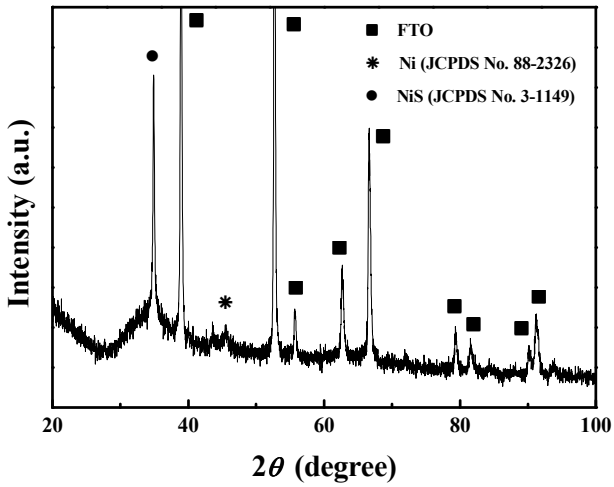

Fig. 3 XRD pattern of a composite film of 200-Ni@NiS.

Journal of Materials Chemistry A Accepted Manuscript

This journal is © The Royal Society of Chemistry [year]

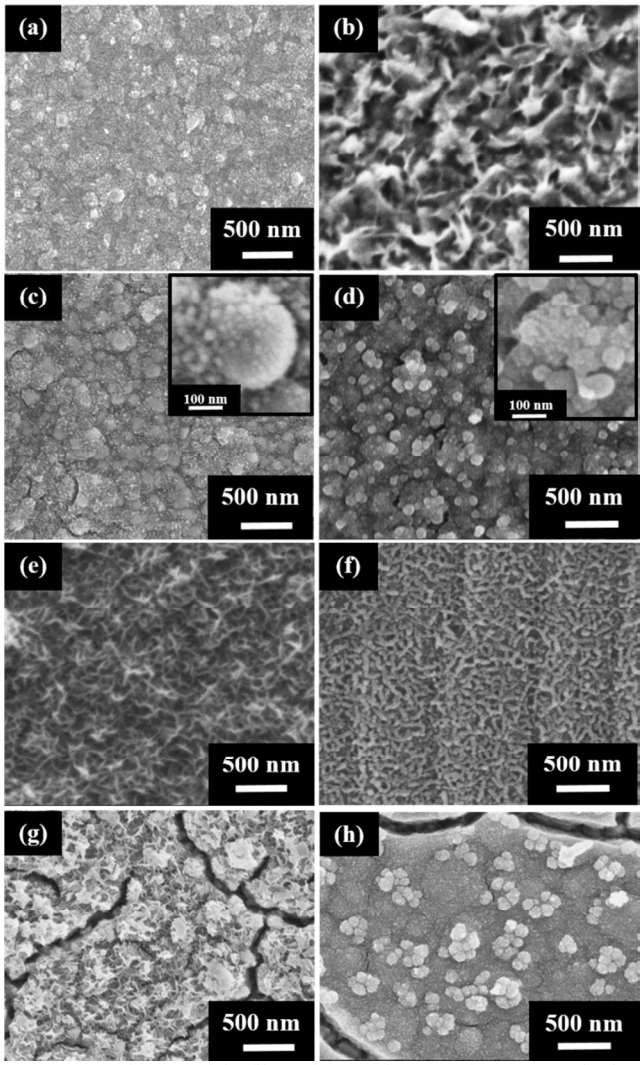

Fig. 4 SEM images of the films of (a) Pt, (b) Bare NiS, (c) 100-Ni, (d) 100-Ni@NiS, (e) 200-Ni, (f) 200-Ni@NiS, (g) 300-Ni, and (h) 300-Ni@NiS.

Fig. 4a shows the image of a platinum film. The Pt film is rather flat and has small and uniform nanoparticles of platinum. Fig. 4b reveals the structure of the bare NiS film. Uniformly distributed flakes of NiS can be seen in the image; the porosity of the film is quite obvious. The length of the flakes appear to be about 500 nm on an average. Fig. 4c depicts the image of 100-Ni, *i.e.*, the image of the nickel layer on the FTO glass, obtained by using 100 mC/cm^2. The magnified image of Fig. 4c indicates the shape of the 100-Ni particle to be a custard apple. We have shown it schematically in Scheme 1a. Fig. 4d shows the image of 100-Ni@NiS composite film, *i.e.*, the composite film obtained by using the 100-Ni film. The inset in it shows its magnified version. It can be seen that the Ni@NiS particle assumed the same shape as that of the particle of Ni, *i.e.*, a custard apple, as also shown in Scheme 1b; this is the same phenomenon found in the case of the composite films, obtained by using the charge densities of 200 mC/cm^2 (200-Ni@NiS) and 300 mC/cm^2 (200-Ni@NiS) for the deposition of their Ni films. For this reason we used the word "Ni template" in this report. The 200-Ni template shows a highly porous coral-like nanostructure in Fig. 4e, which can provide extremely high surface area and also one-dimensional (1D) electron transfer pathways, as sketched in Scheme 1c. The corresponding 200-Ni@NiS composite thin film also exhibits a coral-like nanostructure, however with some regularity in the coral formation (Fig. 4f) and Scheme 1d. In contrast, the 300-Ni template shows a cracked structure in Fig. 4g, as sketched in Scheme 1e. Therefore, deposition of NiS on this Ni template film has resulted in a composite film with similar cracks as those in Ni template film, as shown in Fig. 4h and Scheme 1f.

Photovoltaic performance of the DSSCs with various CEs.

Photocurrent density–voltage (*J–V*) characteristics of the DSSCs with different CEs, with the films of platinum, Bare NiS, 100-Ni@NiS, 200-Ni@NiS, and 300-Ni@NiS were measured at 100 mW cm^{-2}, and are shown in Fig. 5. The corresponding parameters are listed in Table 1. The standard DSSC with Pt counter electrode shows a cell efficiency (η) of 8.11%. The DSSC with Bare NiS exhibits an η of 6.47%. The short-circuit photocurrent densities (J_{sc}) of the DSSCs with 100-Ni@NiS, 200-Ni@NiS, and 300-Ni@NiS are 14.65, 15.36, and 14.78 mA cm^{-2}, respectively. Comparing the SEM images of 100-Ni@NiS (Fig. 4d), 200-Ni@NiS (Fig. 4f), and 300-Ni@NiS (Fig. 4h), it may be said that the coral-like film of 200-Ni@NiS is much more porous than the other two films, and has the largest effective surface area; this could have led to the higher J_{sc} in favor of the cell with the coral-

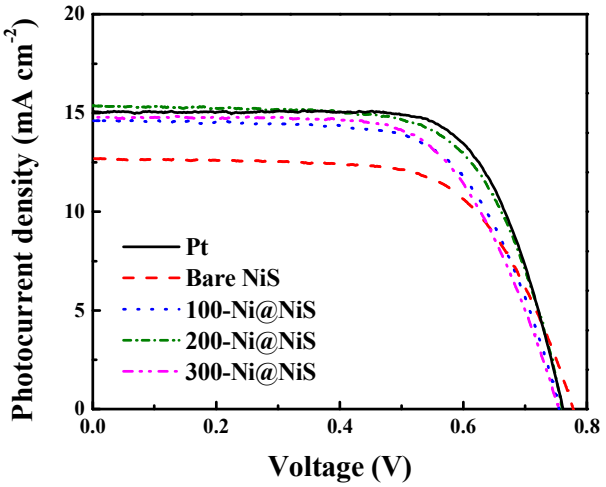

Fig. 5. Photocurrent density–voltage curves of the DSSCs with various CEs measured at 100 mW cm^{-2} (AM 1.5G).

Table 1 Photovoltaic parameters of the DSSCs with various CEs, measured at 100 mW cm^{-2} (AM 1.5G).

Counter electrode	η (%)	V_{OC} (V)	J_{SC}[a] (mA cm^{-2})	*FF*	$J_{SC\text{-}IPCE}$[b] (mA cm^{-2})
Pt	8.11±0.12	0.76±0.01	15.12±0.35	0.70±0.01	15.04
Bare NiS	6.47±0.22	0.78±0.01	12.66±0.46	0.66±0.01	12.02
100-Ni@NiS	7.28±0.13	0.76±0.01	14.65±0.54	0.66±0.01	14.20
200-Ni@NiS	7.84±0.15	0.76±0.01	15.36±0.24	0.68±0.01	15.13
300-Ni@NiS	7.29±0.24	0.75±0.01	14.78±0.37	0.66±0.01	14.26

[a] Values obtained from *J-V* curves; [b] Values obtained from IPCE spectra

Journal of Materials Chemistry A Accepted Manuscript

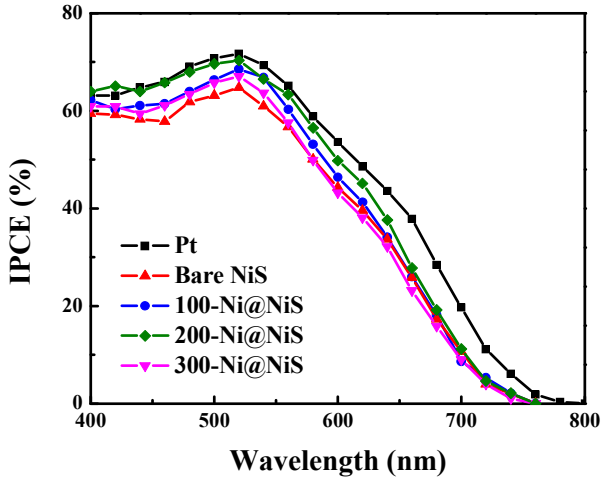

Fig. 6. Incident photon–to–current conversion efficiency curves of the DSSCs with various CEs.

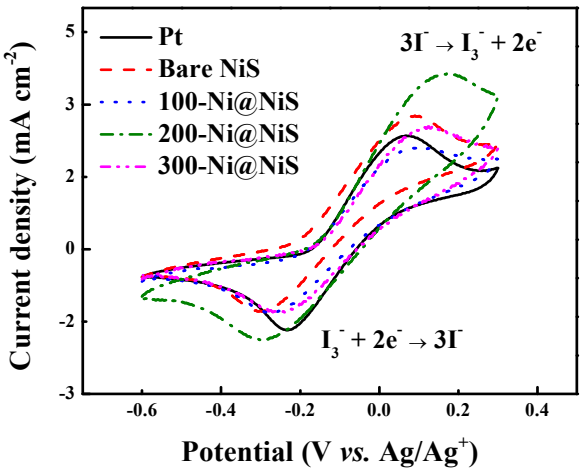

Fig. 7. Cyclic voltammograms of various CEs in an electrolyte containing 10.0 mM LiI, 1.0 mM I_2, and 0.1 M $LiClO_4$ in ACN.

like film of 200-Ni@NiS. Thus, the coral-like 200-Ni@NiS shows the best photovoltaic performance for its DSSC, with an η of 7.84%, while the cell with platinum on its counter electrode shows an η of 8.11%.

We also have performed at-rest long-term test for the DSSC with 200-Ni@NiS as the counter electrode material. In order to eliminate the effect of solvent evaporation, and focus only on the effect of the counter electrode on the stability of the DSSC, a binary ionic liquid electrolyte containing 0.2 M I_2 and 0.5 M TBP in a mixture solvent of BMII/$EMIBF_4$ (volume ratio = 65/35) is used for the test, in accordance with our previous report[34]. As shown in Fig. S1 (page S1, electronic supplementary information), the DSSC with the 200-Ni@NiS CE shows an unfailing long-term stability over a period of one month. It is thus obvious that the 200-Ni@NiS is a stable electrocatalytic film for the CE of a DSSC.

Incident photon-to-current conversion efficiency (IPCE)

IPCE is defined as the number of electrons in the external circuit produced at a given wavelength divided by the number of incident photons. Under a short–circuit condition, the IPCE (λ) value is defined as:

$$IPCE(\lambda) = \frac{1240 \times J_{sc}(\lambda)}{\lambda \times \varphi} \quad (1)$$

where λ is the wavelength, $J_{SC}(\lambda)$ is the short–circuit photocurrent density (mA cm^{-2}), and φ is the incident radiation flux (mW cm^{-2}). The IPCE spectra of cells with various CEs are shown in Fig. 6. A higher IPCE spectrum indicates a higher photocurrent density under short–circuit condition. The maximum IPCE values of the cells with Pt, Bare NiS, 100-Ni@NiS, 200-Ni@NiS, and 300-Ni@NiS are 71.6%, 64.8%, 68.8%, 70.3%, and 66.9% at 520 nm, respectively. The IPCE curves can be utilized to obtain total theoretical current densities ($J_{SC\text{-}IPCE}$), by integrating the areas under the IPCE curves. The thus calculated $J_{SC\text{-}IPCE}$ values, which are shown in Table 1, for the DSSCs with Pt, Bare NiS, 100-Ni@NiS, 200-Ni@NiS, and 300-Ni@NiS CEs are 15.04, 12.02, 14.20, 15.13, and 14.26 mA cm^{-2}, respectively. It can be inferred that the $J_{SC\text{-}IPCE}$ values are in good agreement with the J_{SC} values obtained from the *J-V* curves.

Cyclic voltammetry to analyze electrocatalytic abilities of the counter electrodes

The results obtained from *J-V* curves can be further explained by the data from cyclic voltammetry (CV). The CV analyses can reveal the overall electrocatalytic activities of the counter electrodes. Figure 7 depicts the cyclic voltammograms of the electrodes with various catalytic films. The catalytic reduction reaction at the interface of the counter electrode/electrolyte containing I^-/I_3^- couple can be represented as follows:

$$I_3^- + 2e^- \rightarrow 3I^- \quad (2)$$

It can be seen in Fig. 7 that the catalytic (cathodic) peak current density (I_{pc}) of the electrode with 200-Ni@NiS is the highest, followed by the catalytic current density of the electrode with Pt film. The cathodic peak current densities for all the electrodes are given in Table 2. The I_{pc} values for Pt, Bare NiS, 100-Ni@NiS, 200-Ni@NiS, and 300-Ni@NiS are 1.88, 1.28, 1.51, 1.90, and 1.54 mA cm^{-2}, respectively. The highest value of 1.90 mA cm^{-2} for the counter electrode with 200-Ni@NiS indicates its highest catalytic ability for the reduction of I_3^- ions in the electrolyte. This highest catalytic ability of the counter electrode with 200-Ni@NiS is consistent with the highest J_{SC}, *FF*, and η of its DSSC. We have performed long-term stability test for the electrode with 200-Ni@NiS as the catalytic film by using CV in the same electrolyte mentioned in the experimental section. CV curves of 200-Ni@NiS were obtained for 100 cycles and are shown in the electronic supplementary information (page S2, Fig. S2a). Fig. S2b shows the anodic and cathodic peak current densities as functions of the number of cycles. After 100 cycles, the normalized cathodic and anodic peak current densities remain almost the same, suggesting that the 200-Ni@NiS composite thin film is stable and not corroded in the I^-/I_3^- electrolyte.

Journal of Materials Chemistry A Accepted Manuscript

This journal is © The Royal Society of Chemistry [year]

Conductivities of the counter electrodes

The sheet resistances (R_{sh}), relating the electrical conductivities of the three Ni nano-templates, were obtained by four-point probe method. The R_{sh} values for 100-Ni, 200-Ni, and 300-Ni are 5.89, 3.17, and 8.34 Ω/□, respectively. The thicknesses of the films of 100-Ni, 200-Ni, and 300-Ni are 378, 533, and 896 nm, respectively. This variation in thickness was the result of application of three different charge densities to deposit the Ni templates. With the increase in the charge density from 100 to 300 mC/cm^2, the thickness of nickel film increased gradually. The least value of R_{sh} in the case of 200-Ni film (3.17 Ω/□) may be attributed to its coral-structure with high porosity (Fig. 4e), which would offer 1D electron transfer pathways. The R_{sh} values for 200-Ni@NiS film and Pt film were also measured, and were found to be 7.88 Ω/□ and 7.47 Ω/□, respectively; these values are consistent with the *FF* and *Jsc* values of their pertinent DSSCs (Table 1).

Electrochemical Impedance Spectroscopy

Electrochemical impedance properties of different counter electrodes, namely R_s and R_{ct} are measured by using their symmetric cells, where R_s is the ohmic series resistance and R_{ct} is the charge transfer resistance at the electrode/electrolyte interface. Fig. 8 shows the impedance spectra of the symmetric cells with Pt, Bare NiS, 100-Ni@NiS, 200-Ni@NiS, and 300-Ni@NiS, and Table 2 reports all the *R* values.

The inset in Fig. 8 shows the equivalent circuit. An EIS of a symmetric cell can be divided into three parts. The ohmic series resistance (R_s), is determined in the high frequency region (10^6~10^5 Hz) where the phase is zero. The first semicircle in the middle frequency range (10^5~10 Hz) represents the resistance associated with the heterogeneous electron transfer at the CE/electrolyte interface (R_{ct}). The value of R_s is the resistance value at the onset point of the first semicircle, and the value of R_{ct} is the value of the radius of the first semicircle. Table 2 shows that the values of R_s associated with the counter electrodes of Pt, Bare NiS, 100-Ni@NiS, 200-Ni@NiS, and 300-Ni@NiS are 14.43, 14.07, 17.88, 17.72, and 18.93 Ω cm^2, respectively. It may be noted in Table 2 that the R_s value of the DSSC with Pt is comparable to that of the DSSC with Bare NiS, but lower than those of the DSSCs with Ni@NiS. R_s value corresponds to the series resistance of the symmetric cell, which contains the sheet resistance of the transparent conducting oxide glass and the contact resistance of the cell[40]. In our case, all the Ni@NiS core-shell films have one more contact surface than that of Bare NiS film and of Pt film; this additional contact surface could lead to a higher R_s value for the cell with Ni@NiS, compared to those values of the cells with Bare NiS or Pt. However, the cell performance is affected by various key factors, including surface area, electrocatalytic ability, and conductivity of the counter electrode film. The cells with Ni@NiS all show higher catalytic abilities than that of the cell with Bare NiS. Though the cell with Pt shows a lesser catalytic ability than that of the cell with 200-Ni@NiS, Pt has a higher conductivity than 200-Ni@NiS. These favorable factors have apparently rendered higher efficiencies to the cells with 200-Ni@NiS and Pt. On the other hand, the R_{ct} values of the symmetric cells with Pt, Bare NiS, 100-Ni@NiS, 200-Ni@NiS, and 300-Ni@NiS are 2.88, 7.14, 3.18, 2.47, and 3.21 Ω cm^2, respectively. In absence of the layer of Ni, the symmetric cell with Bare NiS shows a much larger R_{ct} value of 7.14 Ω cm^2, compared to those of the cells with the composite films that have Ni templates (3.18, 2.47, and 3.21 Ω cm^2 for 100-Ni@NiS, 200-Ni@NiS, and 300-Ni@NiS, respectively). The lower J_{sc} value of NiS-DSSC (12.66 mA cm^{-2}), compared to those of the DSSCs with the composite films (14.65, 15.36, and 14.78 mA cm^{-2} for 100-Ni@NiS, 200-Ni@NiS, and 300-Ni@NiS, respectively) is consistent with these R_{ct} values. The lowest R_{ct} value with 200-Ni@NiS enable the highest fill factor, J_{sc}, and η in favor of the cell with 200-Ni@NiS, with reference to these photovoltaic parameters of the cells with the composite films.

Tafel polarization plots

To further investigate the catalytic activities, Tafel polarization curves were obtained for the electrodes with Pt, Bare NiS, 100-Ni@NiS, 200-Ni@NiS, and 300-Ni@NiS, using, in each case, a

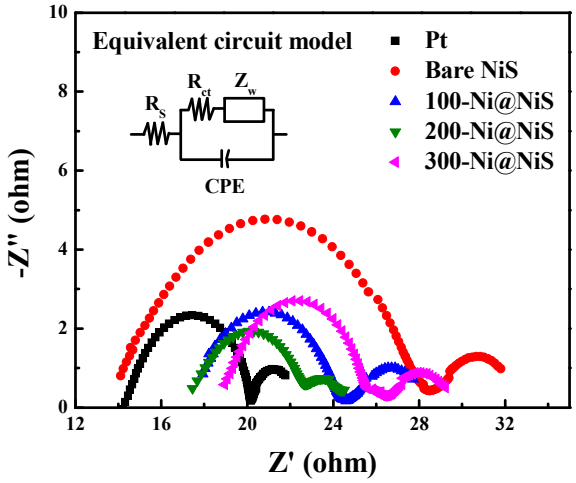

Fig. 8. Electrochemical impedance spectra of various CEs.

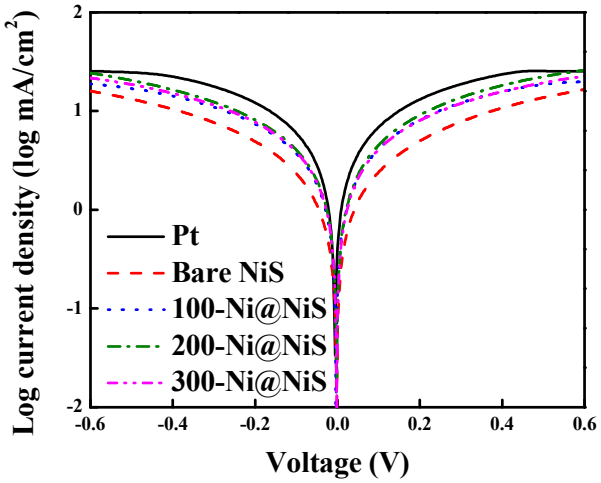

Fig. 9. Tafel polarization plots of various CEs.

Journal of Materials Chemistry A Accepted Manuscript

Table 2 Electrochemical parameters for various counter electrodes.

Counter electrode	I_{pc} (mA cm^{-2})	R_s (Ω cm^2)	R_{ct}[a] (Ω cm^2)	R_{ct}[b] (Ω cm^2)
Pt	1.88	14.43	2.88	2.68
Bare NiS	1.28	14.07	7.14	6.63
100-Ni@NiS	1.51	17.88	3.18	3.20
200-Ni@NiS	1.90	17.72	2.47	2.65
300-Ni@NiS	1.54	18.93	3.21	3.20

[a] Values obtained from EIS; [b] Values obtained from Tafel plots.

symmetrical cell with two identical electrodes. Fig. 9 shows Tafel polarization curves, each presenting logarithmic current density (log I) as a function of voltage (V). Theoretically, there are three zones for each of the Tafel curves; the curve at low potentials (|V| < 120 mV) represents the polarization zone, the one at the middle potentials (with a sharp slope) represents the Tafel zone, and the other at the high potentials (horizontal part) represents the diffusion zone. The slopes of the cathodic and anodic branches of the plots in the Tafel zone for the electrode with 200-Ni@NiS are higher comparable to the corresponding slopes for the electrodes with NiS, 100-Ni@NiS and 300-Ni@NiS; this means that the electrode with 200-Ni@NiS can trigger the reduction of I_3^- to I^- more effectively than the electrodes with NiS, 100-Ni@NiS and 300-Ni@NiS. The exchange current densities can be estimated from the extrapolated intercepts of the anodic and cathodic branches of the corresponding Tafel curves at the exchange current density axes. The values of R_{ct} can also be calculated by using the following relationship between the exchange current density J_0 and R_{ct}: [39]

$$J_0 = \frac{RT}{nFR_{ct}} \quad (3)$$

where R is the gas constant, T is the temperature, F is Faraday's constant, n is the number of electrons involved in the reduction of I_3^- ions to I^- ions at the electrode, and R is the charge transfer resistance (here R_{ct}). The values of R_{ct} obtained from Tafel curves are given in Table 2. It can now be seen in Table 2 that the R_{ct} values obtained from EIS and Tafel plots are nearly the same. It may be concluded that Ni@NiS can be further explored to replace the expensive platinum as the catalytic film for the counter electrode of a DSSC, in view of the fact that it is much cheaper than platinum and its DSSC exhibits as much power conversion efficiency as that of a cell with platinum counter electrode.

Conclusions

A coral-like film of nickel/nickel sulfide (Ni@NiS) was obtained on a conducting glass through an electrochemical pulse method, in which the Ni functioned as a template. Three types of Ni@NiS films were obtained. In each case of the films the particle of the film assumes a core-shell structure. XPS data have revealed the formation of Ni and Ni@NiS films on the FTO glass. The computer data of XPS showed the stoichiometric atomic ratio of Ni to S to be 1:1. XRD pattern has confirmed that the Ni@NiS composite film consists of nickel and nickel sulfide. SEM images reveal that by using the charge densities of 100 mC/cm^2, 200 mC/cm^2, and 300 mC/cm^2 for the deposition of Ni films, the corresponding Ni@NiS films assume, respectively, custard apple-like, coral-like, and cracks-filled structures. SEM images also reveal that the shape of a Ni@NiS particle is the replica of its Ni particle (template). The Ni@NiS coated FTO glasses were used as the counter electrodes for dye-sensitized solar cells. The DSSC with the coral-like Ni@NiS film on its counter electrode exhibits the highest power conversion efficiency of 7.84%, while the DSSC with platinum film on its counter electrode shows an η of 8.11%. Sheet resistances of the composite films and IPCE values of the DSSCs are found to be in good agreement with the photovoltaic parameters of the cells. Theoretical values of J_{sc} of the DSSCs calculated from the IPCE data are found to be consistent with the measured values of the *Jsc*. Cyclic voltammograms reveal that the catalytic current density or the cathodic peak current density of the electrode with 200-Ni@NiS is the highest, followed by the catalytic current density of the electrode with platinum film; the *Jsc* of the corresponding DSSCs are found to agree with these I_{pc} values. The lowest R_{ct} value (EIS values) with 200-Ni@NiS enable the highest fill factor, *Jsc*, and η in favor of the cell with 200-Ni@NiS, with reference to these photovoltaic parameters of the cells with other composite films. Tafel polarization curves reveal that the electrode with 200-Ni@NiS can catalyze the reduction of I_3^- to I^- more effectively than the electrodes with NiS, 100-Ni@NiS and 300-Ni@NiS. The R_{ct} values obtained from EIS and Tafel plots are found to be nearly the same. It may be concluded that Ni@NiS can be further explored to replace the expensive platinum as the catalytic film for the counter electrode of a DSSC, considering the fact that it is much cheaper than platinum and its DSSC exhibits as high power conversion efficiency as that of a cell with platinum counter electrode.

Acknowledgements

This work was sponsored by the National Science Council of Taiwan, under grant number of NSC 102-2221-E-002-186-MY3.

Notes and references

[a]*Department of Chemical Engineering, National Taiwan University, No. 1, Sec. 4, Roosevelt Road, Taipei 10617, Taiwan. Fax: +886–2–2362–3040; Tel: +886–2–2366–0739; E–mail:kcho@ntu.edu.tw*
[b]*Institute of Polymer Science and Engineering, National Taiwan University, No. 1, Sec. 4, Roosevelt Road, Taipei 10617, Taiwan.*
[*] *Corresponding Author: E-mail: kcho@ntu.edu.tw*
[+] *These authors contributed equally*
† Electronic supplementary information (ESI) available. See DOI:10.1039/b000000x/

1. Y. Lin, B. Tan and Y. Wu, *Nano Lett.,* 2007, **8**, 265.
2. C. W. Kung, H. W. Chen, C. Y. Lin, K. C. Huang, R. Vittal and K. C. Ho, *ACS Nano,* 2012, **6**, 7016.
3. L. Y. Chang, C. P. Lee, R. Vittal, J. J. Lin and K. C. Ho, *J. Mater. Chem.,* 2012, **22**, 12305.
4. D. P. Volanti, D. Keyson, L. S. Cavalcante, A. Z. Simões, M. R. Joya, E. Longo, J. A. Varela, P. S. Pizani and A. G. Souza, *J. Alloy. Compd.,* 2008, **459**, 537.

Journal of Materials Chemistry A Accepted Manuscript

This journal is © The Royal Society of Chemistry [year]

5. S. Xu, Y. Luo, Z. Xiao, W. Zhong and Y. Luo, *Electrochim. Acta,* 2013, **114**, 574.
6. O. Rabin, P. R. Herz, Y. M. Lin, A. I. Akinwande, S. B. Cronin and M. S. Dresselhaus, *Adv. Funct. Mater.,* 2003, **13**, 631.
7. Y. Li, D. Xu, Q. Zhang, D. Chen, F. Huang, Y. Xu, G. Guo and Z. Gu, *Chem. Mater.,* 1999, 11, 3433.
8. G. H. Yue, P. X. Yan, X. Y. Fan, M. X. Wang, D. M. Qu, Z. G. Wu, C. Li and D. Yan, *Electrochem. Solid St.,* 2007, **10**, D29.
9. M. Döbbelin, R. Tena-Zaera, P. M. Carrasco, J. R. Sarasua, G. Cabañero and D. Mecerreyes, *J. Polym. Sci. Pol. Chem.,* 2010, **48**, 4648.
10. Q. Li, Z. L. Wang, G. R. Li, R. Guo, L. X. Ding and Y. X. Tong, *Nano lett.,* 2012, **12**, 3803.
11. F. Gong, H. Wang, X. Xu, G. Zhou and Z. S. Wang, *J. Am. Chem. Soc.,* 2012, **134**, 10953.
12. P. Joshi, Z. Zhou, P. Poudel, A. Thapa, X. F. Wu and Q. Qiao, *Nanoscale,* 2012, **4**, 5659.
13. R. Bajpai, S. Roy, N. Kulshrestha, J. Rafiee, N. Koratkar and D. S. Misra, *Nanoscale,* 2012, **4**, 926.
14. S. F. Wang, F. Xie and R. F. Hu, *Sensor. Actuat. B-Chem.,* 2007, **123**, 495.
15. L. M. Lu, L. Zhang, F. L. Qu, H. X. Lu, X. B. Zhang, Z. S. Wu, S. Y. Huan, Q. A. Wang, G. L. Shen and R. Q. Yu, *Biosens. Bioelectron.,* 2009, **25**, 218.
16. Q. Zhang, Y. Liu, Y. Zhang, X. Ji, Y. Tan and Q. Liu, *Mater. Lett.,* 2013, **107**, 337.
17. J. Xiong, X. Dong, Y. Song and Y. Dong, *J. Power Sources,* 2013, **242**, 132.
18. G. H. Yuan, Z. H. Jiang, A. Aramata and Y. Z. Gao, *Carbon,* 2005, **43**, 2913.
19. D. D. Zhao, S. J. Bao, W. J. Zhou and H. L. Li, *Electrochem. Commun.,* 2007, **9**, 869.
20. M. Chiku, Y. Namba, E. Higuchi and H. Inoue, *Electrochemistry,* 2013, **81**, 792.
21. F. Gobal and S. Jafarzadeh, *Anal. Lett.,* 2013, **46**, 2372.
22. M. A. Abdel Rahim, R. M. Abdel Hameed and M. W. Khalil, *J. Power Sources,* 2004, **134**, 160.
23. X. Yan, X. Tong, J. Wang, C. Gong, M. Zhang and L. Liang, *Mater. Lett.,* 2013, **106**, 250.
24. B. O'Regan and M. Grätzel, *Nature,* 1991, **353**, 737.
25. G. Yue, J. Wu, Y. Xiao, M. Huang, J. Lin, L. Fan and Z. Lan, *Electrochim. Acta,* 2013, **92**, 64.
26. M. Al-Mamun, J. Y. Kim, Y. E. Sung, J. J. Lee and S. R. Kim, *Chem. Phys. Lett.,* 2013, **561**, 115.
27. B. Tang, G. Hu, H. Gao and Z. Shi, *J. Power Sources,* 2013, **234**, 60.
28. G. Yue, J. Wu, J. Y. Lin, Y. Xiao, S. Y. Tai, J. Lin, M. Huang and Z. Lan, *Carbon,* 2013, **55**, 1.
29. C. Yuan, S. Guo, S. Wang, L. Liu, W. Chen and E. Wang, *Ind. Eng. Chem. Res.,* 2013, **52**, 6694.
30. M. Wu, X. Lin, Y. Wang, L. Wang, W. Guo, D. Qi, X. Peng, A. Hagfeldt, M. Grätzel and T. Ma, *J. Am. Chem. Soc.,* 2012, **134**, 3419.
31. Y. Hu, Z. Zheng, H. Jia, Y. Tang and L. Zhang, *J. Phys. Chem. C,* 2008, **112**, 13037.
32. Y. C. Wang, D. Y. Wang, Y. T. Jiang, H. A. Chen, C. C. Chen, K. C. Ho, H. L. Chou and C. W. Chen, *Angew. Chem. Int. Ed. Engl.,* 2013, **52**, 6694.
33. L. Yi, Y. Liu, N. Yang, Z. Tang, H. Zhao, G. Ma, Z. Su and D. Wang, *Energ. Environ. Sci.,* 2013, **6**, 835.
34. C. T. Li, C. P. Lee, Y. Y. Li, M. H. Yeh and K. C. Ho, *J. Am. Chem. Soc. A,* 2013, **1**, 14888.
35. G. H. Guai, M. Y. Leiw, C. M. Ng and C. M. Li, *Adv. Energy Mater.,* 2012, **2**, 334.
36. Y. Y. Dou, G. R. Li, J. Song and X. P. Gao, *Phys. Chem. Chem. Phys.,* 2012, **14**, 1339.
37. H. Sun, D. Qin, S. Huang, X. Guo, D. Li, Y. Luo and Q. Meng, *Energ. Environ. Sci.,* 2011, **4**, 2630.
38. Z. Ku, X. Li, G. Liu, H. Wang, Y. Rong, M. Xu, L. Liu, M. Hu, Y. Yang and H. Han, *J. Am. Chem. Soc. A,* 2013, **1**, 237.
39. A. Bard and L. Faulkner, *Electrochemical Methods: Fundamental and Applications*, 2nd ed., John Wiley & Sons, Inc., 2001.
40. Q. Wang, S. Ito, M. Grätzel, F. Fabregat-Santiago, I. Mora-Seró, J. Bisquert, T. Bessho and H. Imai, *J. Phys. Chem. B*, 2006, **110**, 25210.

Journal of Materials Chemistry A Accepted Manuscript